

# Determination of the electronics transfer function for current transient measurements

Christian Scharf\*, Robert Klanner

*Institute for Experimental Physics, University of Hamburg, Germany*

---

## Abstract

We describe a straight-forward method for determining the transfer function of the readout of a sensor for the situation in which the current transient of the sensor can be precisely simulated. The method relies on the convolution theorem of Fourier transforms. The specific example is a planar silicon pad diode. The charge carriers in the sensor are produced by picosecond lasers with light of wavelengths of 675 and 1060 nm. The transfer function is determined from the 1060 nm data with the pad diode biased at 1000 V. It is shown that the simulated sensor response convoluted with this transfer function provides an excellent description of the measured transients for laser light of both wavelengths. The method has been applied successfully for the simulation of current transients of several different silicon pad diodes. It can also be applied for the analysis of transient-current measurements of radiation-damaged solid state sensors, as long as sensor properties, like high-frequency capacitance, are not too different.

*Keywords:* silicon pad sensor, transient current technique, transfer function, Fourier transform

---

*Introduction.* The analysis of current transients from different sensors is frequently limited by the knowledge of the electronics response, which is also influenced by the sensor properties. Examples for silicon sensors are the determination of the electric fields, carrier lifetimes and charge multiplication in radiation-damaged sensors using the Transient Current Technique (TCT, edge-TCT) [1–3] or charged particles with shallow incident angles [4]. The aim of this Technical Note is to demonstrate that, for an experiment in which the pulse shape from the sensor can be precisely simulated, the electronics transfer function can be obtained from the measured transient using the convolution theorem of Fourier transforms. This transfer function can then be used for analyzing data for which the pulse shape of the sensor is not known. An example is the analysis of measured transients from a radiation-damaged sensor using the known transfer function obtained from the sensor before irradiation, as long as detector properties, like the high-frequency capacitance, do not change too much with irradiation.

*Measurement set-up.* The measurement set-up used is described in detail in [5–7]. The measurements have been performed on  $p^+nn^+$  and  $n^+pp^+$  pad diodes with different doping, thicknesses of 200  $\mu\text{m}$  and 285  $\mu\text{m}$ , and 4.4  $\text{mm}^2$  and 25  $\text{mm}^2$  area. In all cases the electronics response function has been successfully determined. Here we present the results from a  $p^+nn^+$  pad diode produced by Hamamatsu [8] on a  $\langle 100 \rangle$  crystal with 204.5  $\mu\text{m}$  mechanical thickness, 4.4  $\text{mm}^2$  area, and  $2.9 \cdot 10^{12} \text{ cm}^{-3}$  phosphorous doping, which was connected by a 3 m long RG58 cable and a bias-T to an amplifier [9], and read out by a Tektronix DPO 4104 oscilloscope with a bandwidth of 1 GHz and a sampling rate of 5 GS/s. A guard ring was present but not connected for the measurements. The active thickness of the pad diode was estimated to  $200 \pm 1 \mu\text{m}$  from dielectric as well as caliper measurements of the physical thickness minus the thickness of the implants from

---

\*Corresponding author. Email address: Christian.Scharf@desy.de, Telephone: +49 40 8998 4725.

29 spreading resistance measurements [10]. The depletion voltage was determined to  $87.5 \pm 3.0$  V,  
 30 from capacitance measurements with a capacitance above the depletion voltage of about 2.7 pF.

31 The charge carriers were generated by picosecond lasers [11] pulsed at a frequency of 200 Hz  
 32 with a full-width-at-half-maximum of less than 50 ps and wavelengths of 675 and 1060 nm. For  
 33 each pulse approximately  $10^6$  electron-hole pairs were generated, and for every measurement 512  
 34 pulses were averaged. At room temperature the absorption length in silicon for light of 1060 nm is  
 35 about 1.5 mm. As the attenuation length is long compared to the sensor thickness, the distribution  
 36 of charge carriers is similar as for charged particles traversing the sensor. At this wavelength the  
 37 absorption length is a strong function of temperature [12, 13]. It is about  $650 \mu\text{m}$  at  $40^\circ\text{C}$ . The  
 38 absorption length for light of 675 nm is about  $3.3 \mu\text{m}$  at room temperature, and the signal induced  
 39 in the electrodes of the sensor is essentially due to electrons if the light is injected at the  $p^+$  side,  
 40 and due to holes if injected at the  $n^+$  side.

41 *Simulations.* In the simulations a uniform doping in the active region of the sensor is assumed,  
 42 resulting in a linear position dependence of the electric field. Using the field simulated with  
 43 SYNOPSIS-TCAD [14] which includes realistic doping distributions at the  $p^+n$  and  $n^+n$  transi-  
 44 tions [15], it has been checked that the current transients for voltages 50 V above the depletion  
 45 voltage are hardly affected by the electric field distribution at the transitions.

46 Electrons and holes are generated on a grid with 100 nm spacing according to exponentials  
 47 with the light-absorption lengths given above. The charge carriers are then drifted in the electric  
 48 field in time steps  $\Delta t = 10$  ps taking into account diffusion by Gaussians with variances  $\sigma_e =$   
 49  $\sqrt{(2 \cdot \mu_e \cdot k_B T / q_0) \Delta t}$  for electrons, and similar for holes, with the Boltzmann constant  $k_B$ , the  
 50 absolute temperature  $T$ , the elementary charge  $q_0$ , and the electron and hole mobilities  $\mu_e$  and  
 51  $\mu_h$ . The field dependence of the mobilities of electrons and holes was adjusted to describe our  
 52 measurements [5, 16]. The main difference compared to the standard parametrization [17] is that  
 53 at high fields ( $\approx 50$  kV/cm) the electron and the hole drift velocities are similar. We note that there  
 54 are hardly any measurements of the drift velocities for  $\langle 100 \rangle$  silicon available. The current induced  
 55 in the electrodes in the time interval between  $i \cdot \Delta t$  and  $(i + 1) \cdot \Delta t$  is calculated according to  
 56  $I_i^{sim} = q_0 / \Delta t \cdot \sum_j [(N_{i+1,j}^e - N_{i,j}^e) - (N_{i+1,j}^h - N_{i,j}^h)]$ , where  $N_{i,j}^e$  is the number of electrons and  
 57  $N_{i,j}^h$  the number of holes at the grid point  $j$  at time  $i \cdot \Delta t$ . Effects like charge trapping or charge  
 58 multiplication are not taken into account. The convoluted signal is given by  $S_k^{sim} = \sum_l I_{k-l}^{sim} \cdot R_l$ ,  
 59 where  $R_l$  is the response at  $t = l \cdot \Delta t$  to an initial unit current at  $t = 0$ .

60 *Transfer function determination.* The measurements have been performed for voltages between  
 61 100 V and 1000 V in steps of 10 V. For every voltage three sets of data were taken: 1060 nm light  
 62 injected from the  $p^+$  side, called "IR", 675 nm light injected from the  $p^+$  side, "e", and 675 nm  
 63 light injected from the  $n^+$  side, "h". For "IR" holes and electrons contribute equally to the signal,  
 64 whereas for "e" electrons, and for "h" holes dominate. For determining the transfer function  $R$ , the  
 65 IR measurement at 1000 V is used. A spline interpolation of the measurement  $I^{int}$  is used to obtain  
 66 values for the same time steps  $\Delta t = 10$  ps as in the simulation. Next the Fast Fourier Transforms  
 67  $\mathcal{F}(I^{sim})$  and  $\mathcal{F}(I^{int})$  are calculated, and the transfer function is obtained by  $R = \mathcal{F}^{-1}[\mathcal{F}(I^{int}) / \mathcal{F}$   
 68  $(I^{sim})]$ , using the well-known convolution theorem  $\mathcal{F}(f \otimes g) = \mathcal{F}(f) \cdot \mathcal{F}(g)$ .

69 Fig. 1 shows the elements used in the determination of the transfer function  $R$ : the spline-  
 70 interpolated measured current transient  $I^{int}$ , the simulated current transient before convolution  
 71  $I^{sim}$ , and  $R$  obtained as described. As shown in Fig. 3 the transients for electrons and holes at  
 72 1000 V are very similar implying that at high fields around 50 kV/cm the drift velocities of electrons  
 73 and holes are also similar. As a result,  $I^{sim}$  for IR at 1000 V, which is a superposition of electron  
 74 and hole drift, is to a good approximation a straight line without a tail from slower holes. The  
 75 time step for all curves is 10 ps. The time shift between the simulated and the measured transient  
 76 is arbitrary. It does not change the shape of  $R$ , but just its position along the time axis.

77 *Comparison of measurements with simulations.* Fig. 2 compares the current transient for the IR  
 78 measurement at 1000 V with the simulated transient using for the convolution the transfer function  
 79 determined from the same data. For the simulation only the values at the times at which data were

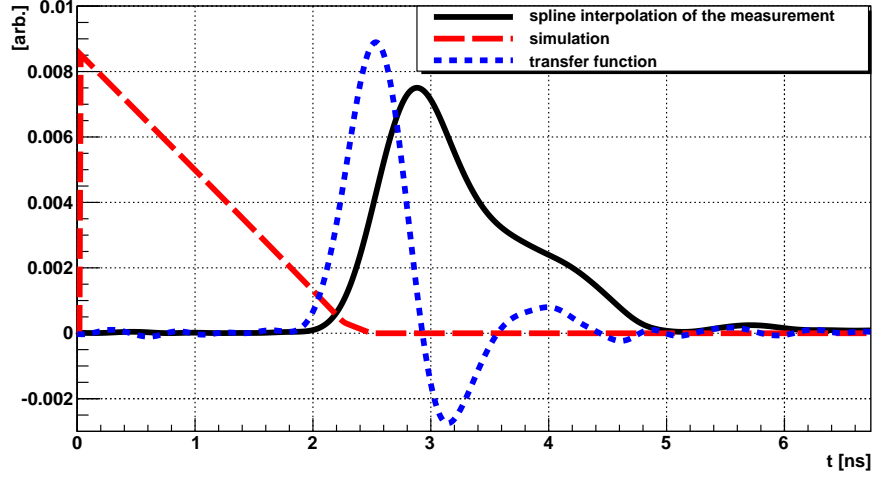


Figure 1: Determination of the transfer function  $R$  (blue dots) from the spline interpolation of the measured transient  $I^{int}$  (black solid) and the simulated transient  $I^{sim}$  (red dashed) for the signal of electrons and holes produced by 1060 nm laser light ( $IR$ ) at 1000 V.

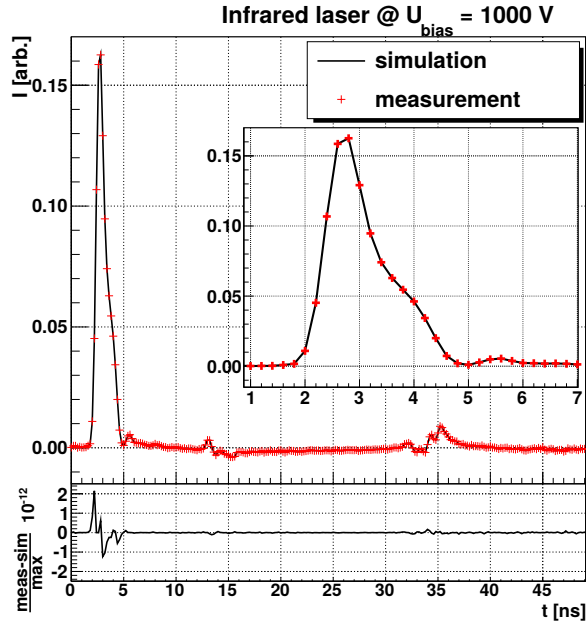


Figure 2: Comparison of the measured current transient (crosses) with the simulated one (solid line) for  $IR$  at 1000 V. The transfer function used for the convolution has been determined from this measurement.

80 recorded are shown. Both the main pulse, shown as insert, as well as the signal reflections are well  
 81 described. The difference between the measured and the simulated signal divided by the maximum  
 82 value of the measured signal is shown at the bottom. Its absolute value is smaller than  $10^{-11}$ . This  
 83 demonstrates the consistency of the method used for determining the electronics transfer function.

84 Fig. 3 compares the current transients for the  $e$  and for the  $h$  measurement at 1000 V with  
 85 the simulated transients using for the convolution the transfer function determined from the  $IR$   
 86 measurement at 1000 V. We note that the transients are very similar and that the  $h$  pulse is only  
 87 slightly longer than the  $e$  pulse. At 1000 V the electric field in the sensors varies between 46 kV/cm

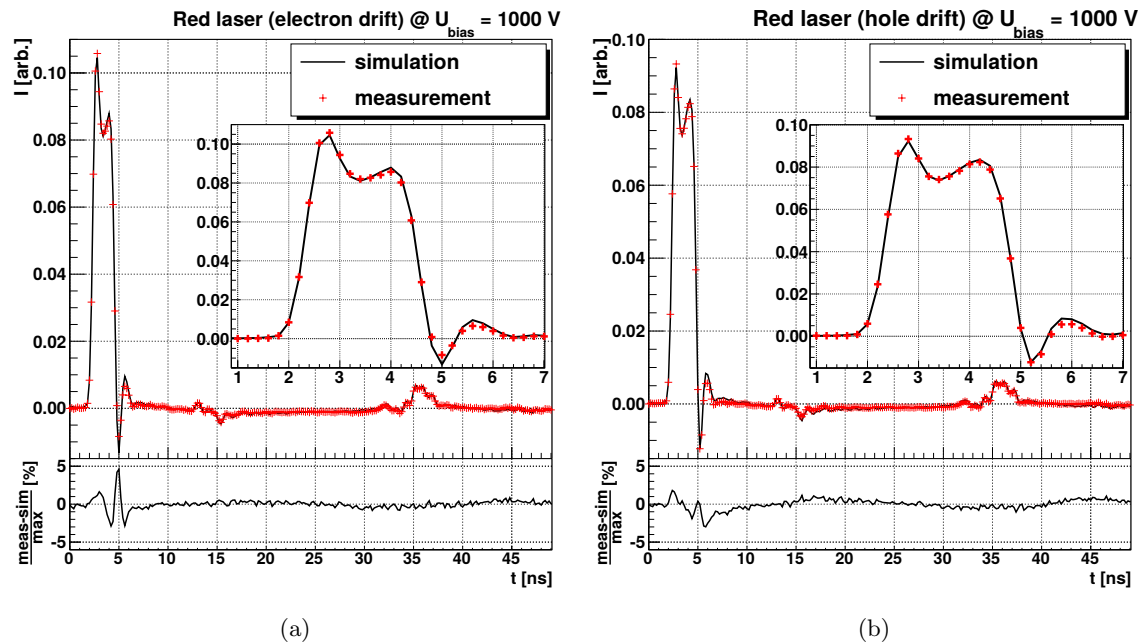


Figure 3: Comparison of the measured current transients (crosses) with the simulated ones (solid lines) at 1000 V using the same transfer function for the convolution as in Fig. 2 for (a) electrons, and (b) holes.

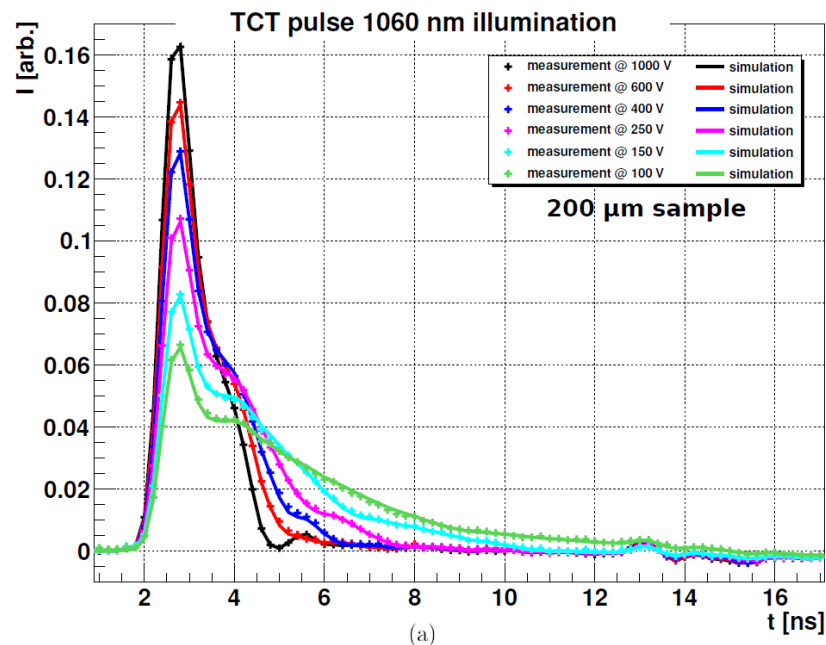


Figure 4: Current transients measured (crosses) and simulated (solid lines) for different bias voltages for 1060 nm laser light.

88 and 54 kV/cm. We conclude that for  $\langle 100 \rangle$  silicon the drift velocities of electrons and holes at  
 89 these high fields are similar with little dependence on the electric field. The difference between  
 90 the measured and the simulated signal divided by the maximum value of the measured signal is  
 91 displayed at the bottom. Its absolute value is less than 5%. This difference provides an idea of the

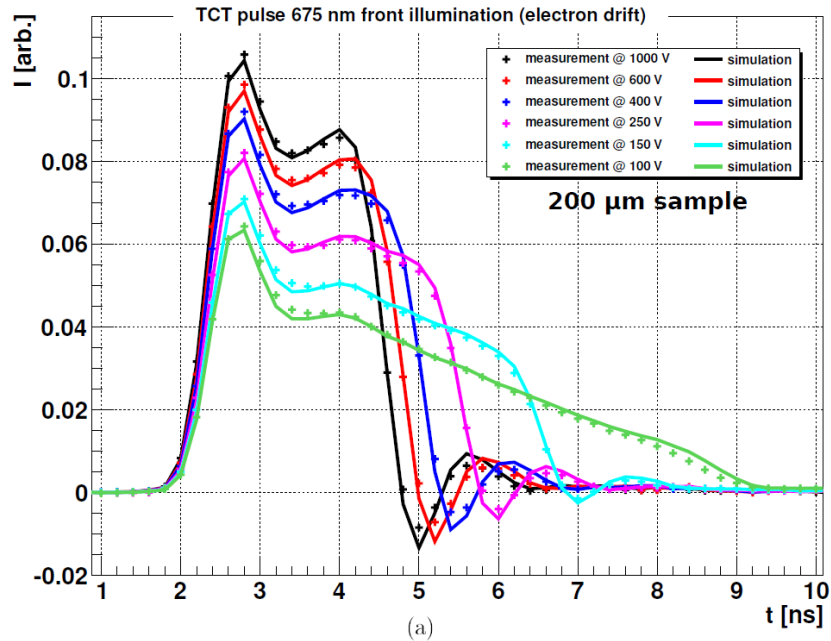


Figure 5: Current transients measured (crosses) and simulated (solid lines) for different bias voltages for 675 nm laser light injected from the  $p^+$  side.

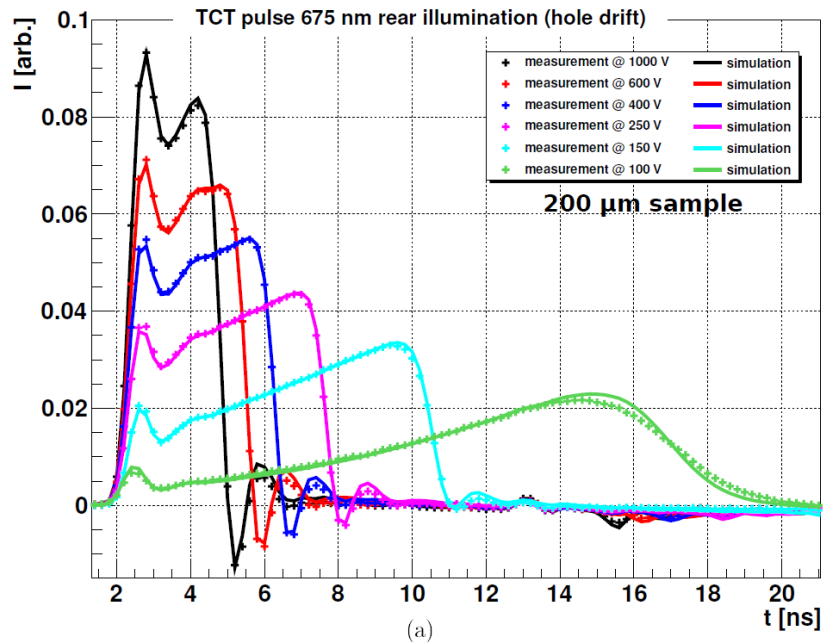


Figure 6: Current transients measured (crosses) and simulated (solid lines) for different bias voltages for 675 nm laser light injected from the  $n^+$  side.

92 accuracy of the simulation and the method used for determining the transfer function since the  
 93 simulated transient before convolution for  $IR$  is significantly different compared to the ones for  $e$   
 94 and  $h$  which are to first approximation boxcar functions.

95 Fig. 4 compares the measured with the simulated current transients for bias voltages between  
 96 100 and 1000 V for  $IR$ . It is seen that for all voltages the data are well described by the simulation.

97 Fig. 5 compares the measured with the simulated current transients for bias voltages between  
 98 100 and 1000 V for  $e$ . With the exception of the 100 V data, the data are well described by the  
 99 simulations. The biasing voltage of 100 V is only 12.5 V above the depletion voltage, and the effect  
 100 of the  $p^+n$  junction where the charges are generated, and of the  $n^+n$  transition, which the electrons  
 101 reach at the higher drift times, may be significant.

102 Fig. 6 compares the measured with the simulated current transients for bias voltages between  
 103 100 and 1000 V for  $h$ . Again, with the exception of the 100 V data, the data are well described by  
 104 the simulations. At 100 V the electron-hole pairs are generated by the laser light in the low-field  
 105 region of the sensor. As the density of the generated electron-hole pairs of  $5 \cdot 10^{12} \text{ cm}^{-3}$  is similar  
 106 to the doping density, the so called plasma effect [18, 19] is expected to occur at low bias voltages.  
 107 The plasma effect is due to the shielding of the sensor field by the counter field of the overlapping  
 108 electron-hole clouds which results in a delayed charge collection. In the simulations the plasma  
 109 effect is not included. We note that the measured current transients for voltages between 150 and  
 110 1000 V are well described by the simulations using the transfer function determined by the method  
 111 described in the paper from the measurement with 1060 nm laser light at 1000 V.

112 The transfer functions have also been determined for the  $\langle 100 \rangle$  silicon pad diodes with different  
 113 thicknesses and capacitances mentioned on page 1. It is found that, although there are significant  
 114 differences in the transfer functions, the measurements can be well described with consistent values  
 115 for the field dependence of the electron and hole mobilities. This demonstrates the validity of the  
 116 proposed method of determining electronic transfer functions.

117 *Practical aspects of the determination of the transfer function.* We conclude the manuscript with  
 118 a few comments on the experience we made, when we developed the method of determining the  
 119 transfer function described in this Technical Note. Initially we used a SPICE simulation of detector,  
 120 cables and readout electronics. Details are given in Ref. [7], where it is also shown that a number  
 121 of parasitic elements had to be included in the simulation to achieve an acceptable description of  
 122 the measurements. However, the results never have been fully satisfactory especially for diodes  
 123 with a capacitance above full depletion below 10 pF. We then used the method described here and  
 124 obtained satisfactory results from the beginning. To better understand the method and its possible  
 125 applications, the following studies have been made.

126 As we do not know, if the current recorded by the oscilloscope is the instantaneous current  
 127 or the current averaged over the sampling interval, the difference between a simulation using the  
 128 value at the bin center and the average value has been investigated. Differences were observed at  
 129 the maxima and minima of the transients, however, they are smaller than 1.5 % of the maximum  
 130 signal and do not change significantly the results of the analyses.

131 For the Fast-Fourier-Transform of the spline-interpolated measurement  $I^{int}$  we included 2 ns  
 132 of the measurement before the pulse has reached 10 % of the maximum. Additionally, we had to  
 133 add at least 3 bins (30 ps) which are set to zero at the start of  $I^{int}$ . Otherwise, we sometimes  
 134 experienced oscillations in the transfer function.

135 We have investigated which of our data should be used for obtaining the optimal transfer  
 136 function. We find that the best overall description of the complete data set is obtained, if the  $IR$   
 137 measurement at 1000 V is used. Our explanation is that the uncertainties of the simulation are  
 138 smallest for these conditions. At the  $n^+n$  and  $p^+n$  sides, there are shallow non-depleted regions  
 139 as well as high-field regions from the doping gradients, which have not been taken into account  
 140 in the simulation. For the red laser a significant fraction of the  $eh$  pairs is generated in these  
 141 regions, whereas for the infrared laser the charges are generated throughout the sensor. In addition,  
 142 at 1000 V the electric field in the 200  $\mu\text{m}$  thick sensor is high; therefore, the variations of the  
 143 drift velocities, which approach the saturation velocities, are minimal. We conclude: The precise  
 144 simulation of the transient induced in electrodes of the sensor is one necessary condition for the  
 145 successful application of the proposed method.

146 Next we discuss the requirements for noise and sampling frequency. Ideally the sampling step  
 147 should be small compared to the width of the transfer function. In our example, however, the  
 148 sampling step of 200 ps is not much shorter than the measured rise time of about 600 ps. As the  
 149 simulated rise time of the current induced in the electrodes is much shorter, the measured rise

150 time is approximately equal to the width of the main peak of the transfer function. However, if  
 151 the noise of the transient measurement is small, which has been achieved by injecting  $10^6$   $eh$  pairs  
 152 per pulse and averaging 512 pulses, an interpolation of the measurements can give reliable results.  
 153 We have used a 5th order spline interpolation for obtaining data in 10 ps steps from the measured  
 154 transients which were recorded in 200 ps steps. Thus, the second necessary condition for a successful  
 155 application of the proposed method are a high signal-to-noise ratio and sampling steps shorter  
 156 than the rise time of the transient.

157 Last but not least: the transfer function, which has been determined from a measurement for  
 158 which the intrinsic detector response could be simulated precisely, can only be used for analyzing  
 159 data from a sensor with similar parameters, with the capacitance being the most important one.

## 160 Acknowledgments

161 We would like to thank Julian Becker for making available his program which simulates the  
 162 current transients in silicon pad diodes and for many helpful discussions, Jörn Schwandt for making  
 163 the TCAD simulations of the electric field which takes into account the  $p^+n$  and  $n^+n$  transition  
 164 regions, and Erika Garutti and Ulrich Koetz, who proof-read the manuscript and made valuable  
 165 suggestions. We are also grateful to the HGF Alliance *Physics at the Terascale* which had funded  
 166 the TCT set-up used for the measurements.

## 167 Bibliography

## 168 References

- 169 [1] G. Kramberger, V. Cindro, I. Mandic, M. Mikuž, M. Milovanović, M. Zavrtanik, and K. Žagar. Investigation of  
 170 irradiated silicon detectors by edge-tct. *Nuclear Science, IEEE Transactions on*, 57(4):2294–2302, Aug 2010.
- 171 [2] M. Mikuž, V. Cindro, G. Kramberger, I. Mandić, and M. Zavrtanik. Study of anomalous charge collection  
 172 efficiency in heavily irradiated silicon strip detectors. *Nuclear Instruments and Methods in Physics Research*  
 173 *Section A: Accelerators, Spectrometers, Detectors and Associated Equipment*, 636(1, Supplement):S50 – S55,  
 174 2011. 7th International Hiroshima Symposium on the Development and Application of Semiconductor Tracking  
 175 Detectors.
- 176 [3] N. Pacifico, I. D. Kittelmann, M. Fahrner, M. Moll, and O. Militaru. Characterization of proton and neutron  
 177 irradiated low resistivity p-on-n magnetic czochralski ministrip sensors and diodes. *Nuclear Instruments and*  
 178 *Methods in Physics Research Section A: Accelerators, Spectrometers, Detectors and Associated Equipment*,  
 179 658(1):55 – 60, 2011. {RESMDD} 2010.
- 180 [4] M. Swartz, V. Chiochia, Y. Allkofer, D. Bortoletto, L. Cremaldi, S. Cucciarelli, A. Dorokhov, C. HÄrmann,  
 181 D. Kim, M. Konecki, D. Kotlinski, K. Prokofiev, C. Regenfus, T. Rohe, D.A. Sanders, S. Son, and T. Speer.  
 182 Observation, modeling, and temperature dependence of doubly peaked electric fields in irradiated silicon  
 183 pixel sensors. *Nuclear Instruments and Methods in Physics Research Section A: Accelerators, Spectrometers,*  
 184 *Detectors and Associated Equipment*, 565(1):212 – 220, 2006. Proceedings of the International Workshop  
 185 on Semiconductor Pixel Detectors for Particles and Imaging {PIXEL} 2005 International Workshop on  
 186 Semiconductor Pixel Detectors for Particles and Imaging.
- 187 [5] C. Scharf. *Measurement of the drift velocities of electrons and holes in high-ohmic <100> silicon*. MSc thesis,  
 188 University of Hamburg, Feb. 2014. DESY-THESIS-2014-015.
- 189 [6] J. Becker, E. Fretwurst, and R. Klanner. Measurements of charge carrier mobilities and drift velocity saturation  
 190 in bulk silicon of <111> and <100> crystal orientation at high electric fields. *Solid-State Electronics*, 56(1):104 –  
 191 110, 2011.
- 192 [7] J. Becker. *Signal development in silicon sensors used for radiation detection*. PhD thesis, University of  
 193 Hamburg, 2010. DESY-THESIS-2010-33.
- 194 [8] Hamamatsu Photonics K.K. <http://www.hamamatsu.com/>.
- 195 [9] Phillips Scientific Fast Pulse Amplifier Model 6954 with some modifications. <http://www.phillipsscscientific.com/pdf/6954ds.pdf/>.
- 196 [10] W. Treberspurg, T. Bergauer, M. Dragicevic, and B. Lutzer. Analysis of test structures and process technology.  
 197 HEPHY Vienna, 2013. Workshop on Silicon Strip Sensors for the CMS Phase II Upgrade.
- 198 [11] Advanced Laser Diode Systems A.L.S. GmbH. Picosecond Injection Laser; (PiLas) Owner’s Manual. <http://alsgmbh.de/>.
- 199 [12] S.M. Sze and Kwok K. Ng. *Photodetectors and Solar Cells*, pages 663–742. John Wiley & Sons, Inc., 2006.
- 200 [13] G. Kramberger. *Signal development in irradiated silicon detectors*. PhD thesis, University of Ljubljana, 2001.
- 201 [14] SYNOPSIS-TCAD. <http://www.synopsys.com/Tools/TCAD/>.
- 202 [15] Jörn Schwandt. Private communication.

- 205 [16] C. Scharf and R. Klanner. Measurement of the drift velocities of electrons and holes in high-ohmic (100)  
206 silicon. *to be submitted to Nuclear Instruments and Methods in Physics Research Section A: Accelerators,*  
207 *Spectrometers, Detectors and Associated Equipment.*
- 208 [17] C Jacoboni, C Canali, G Ottaviani, and A Alberigi Quaranta. A review of some charge transport properties of  
209 silicon. *Solid-State Electronics*, 20(2):77–89, 1977.
- 210 [18] R.N. Williams and E.M. Lawson. The plasma effect in silicon semiconductor radiation detectors. *Nuclear*  
211 *Instruments and Methods*, 120(2):261 – 268, 1974.
- 212 [19] J. Becker, K. Gärtner, R. Klanner, and R. Richter. Simulation and experimental study of plasma effects  
213 in planar silicon sensors. *Nuclear Instruments and Methods in Physics Research Section A: Accelerators,*  
214 *Spectrometers, Detectors and Associated Equipment*, 624(3):716 – 727, 2010.